AD-A190 210 ELECTROMAGNETIC SENSOR ARRAYS FOR NONDESTRUCTIVE EVALUATION AND ROBOT CONTROL(U) SRI INTERNATIONAL MENLO PARK CA A J BAHR ET AL. OCT 87 AFOSR-TR-87-1752 1/1

UNCLASSIFIED F49620-84-K-0011 F/G 17/11 NL

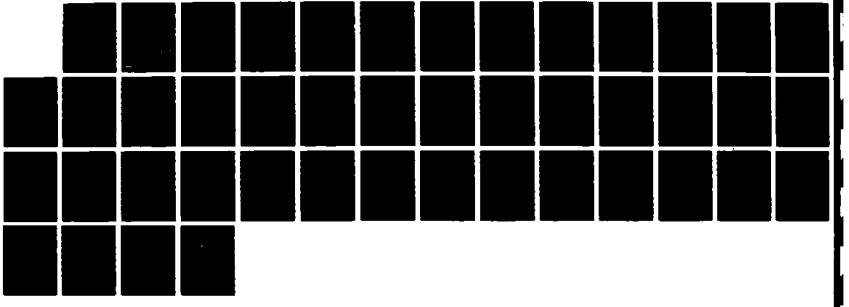

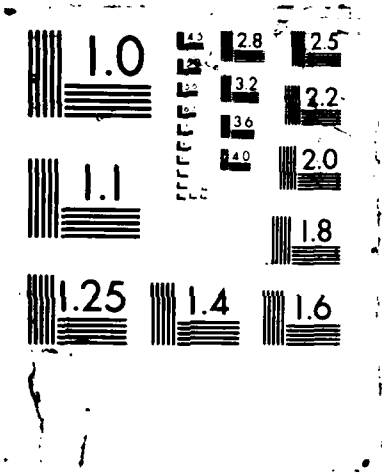
1.0
1.1
1.25
1.4
1.6
1.8
2.0
2.2
2.5
2.8
3.2
3.6
4.0

(2)

AFOSR-TR- 87-1752

Final Annual Report
Covering the Period 1 September 1986 - 31 August 1987

October 1987

ELECTROMAGNETIC SENSOR ARRAYS FOR NONDESTRUCTIVE EVALUATION AND ROBOT CONTROL

By: A. J. Bahr A. Rosengreen

Prepared for:

Air Force Office of Scientific Research
Directorate of Electronic and Solid State Sciences
Bolling Air Force Base, Building 410
Washington, D.C. 20332

Attention: Dr. H. Weinstock
Program Manager, AFOSR/Electronic & Materials Sciences

Contract F49620-84-K-0011

SRI Project 7711

SRI INTERNATIONAL
333 Ravenswood Avenue
Menlo Park, California 94025
(415) 326-6200
Cable: SRI INTL MPK
TWX: 910-373-2046

SRI International®

SRI International

Final Annual Report
Covering the Period 1 September 1986 - 31 August 1987

October 1987

ELECTROMAGNETIC SENSOR ARRAYS FOR NONDESTRUCTIVE EVALUATION AND ROBOT CONTROL

By: A. J. Bahr A. Rosengreen

Prepared for:

Air F ce Office of Scientific Research
Directorate of Electronic and Solid State Sciences
Bolling Air Force Base, Building 410
Washington, D.C. 20332

Attention: Dr. H. Weinstock
Program Manager, AFOSR/Electronic & Materials Sciences

Contract F49620-84-K-0011

SRI Project 7711

Approved by:

TAYLOR W. WASHBURN, *Director*
Remote Measurements Laboratory

LAWRENCE E. SWEENEY, JR., *Vice President*
System Technology Division

SRI INTERNATIONAL, 333 Ravenswood Avenue, Menlo Park, California 94025
(415) 326-6200, Cable: SRI INTL MPK, TWX: 910-373-2046

UNCLASSIFIED

SECURITY CLASSIFICATION OF THIS PAGE

REPORT DOCUMENTATION PAGE

1a. REPORT SECURITY CLASSIFICATION UNCLASSIFIED	1b. RESTRICTIVE MARKINGS NONE
2a. SECURITY CLASSIFICATION AUTHORITY	3. DISTRIBUTION/AVAILABILITY OF REPORT APPROVED FOR PUBLIC RELEASE; DISTRIBUTION UNLIMITED
2b. DECLASSIFICATION/DOWNGRADING SCHEDULE	
4. PERFORMING ORGANIZATION REPORT NUMBER(S) FINAL ANNUAL REPORT, Project 7711	5. MONITORING ORGANIZATION REPORT NUMBER(S) AFOSR-TR- 87-1752
6a. NAME OF PERFORMING ORGANIZATION SRI INTERNATIONAL 6b. OFFICE SYMBOL (if applicable)	7a. NAME OF MONITORING ORGANIZATION Same as 8a ~~CONTRACT NO. F49620-84-K-0011~~
6c. ADDRESS (City, State, and ZIP Code) 333 RAVENSWOOD AVENUE MENLO PARK, CA 94025	7b. ADDRESS (City, State, and ZIP Code) Same as 8c
8a. NAME OF FUNDING/SPONSORING ORGANIZATION USAF, AFSC 8b. OFFICE SYMBOL (if applicable) AFOSR/NE	9. PROCUREMENT INSTRUMENT IDENTIFICATION NUMBER F49620 84-K-0011
8c. ADDRESS (City, State, and ZIP Code) Building 410 Bolling AFB, DC 20332	10. SOURCE OF FUNDING NUMBERS PROGRAM ELEMENT NO. ~~F08671-8401392~~ 61102F PROJECT NO. 2306/~~A2~~ TASK NO. A3 WORK UNIT ACCESSION NO

11. TITLE (Include Security Classification)

Electromagnetic Sensor Arrays for Nondestructive Evaluation & Robot Control

12. PERSONAL AUTHOR(S)

A.J. Bahr and A. Rosengreen

13a. TYPE OF REPORT	13b. TIME COVERED	14. DATE OF REPORT (Year, Month, Day)	15. PAGE COUNT
FINAL ANNUAL	FROM 860901 TO 870831	1987 OCTOBER	40

16. SUPPLEMENTARY NOTATION

17. COSATI CODES			18. SUBJECT TERMS (Continue on reverse if necessary and identify by block number)
FIELD	GROUP	SUB-GROUP	
09	01		Sensor, arrays, nondestructive evaluation, robotics, electromagnetic, imaging, edge tracking

19. ABSTRACT (Continue on reverse if necessary and identify by block number)

The objective of this research program was to develop the theoretical models, design methodology, and technology needed for optimally applying near-field electromagnetic sensor arrays to nondestructive evaluation (NDE) and robot control. This program was a collaborative effort by SRI International and Stanford University. This report summarizes SRI's contribution to the program's third-year research activities.

SRI's work on this study has shown that small printed-circuit single-turn loops exhibit good sensitivity when used as sensors. This technology allows ready fabrication of high-resolution arrays. By addressing different elements in the array and suitably processing the resulting signals, different sensing functions can be realized with the same array. In particular, SRI has demonstrated the use of such arrays for edge tracking and ranging (proximity sensing).

20. DISTRIBUTION AVAILABILITY OF ABSTRACT	21. ABSTRACT SECURITY CLASSIFICATION	
☐ UNCLASSIFIED/UNLIMITED ☒ SAME AS RPT ☐ DTIC USERS	UNCLASSIFIED	
22a. NAME OF RESPONSIBLE INDIVIDUAL Dr. H. Weinstock	22b. TELEPHONE (Include Area Code) (207) 767-4933	22c. OFFICE SYMBOL AFOSR/NE

DD FORM 1473, 84 MAR

83 APR edition may be used until exhausted
All other editions are obsolete

SECURITY CLASSIFICATION OF THIS PAGE

UNCLASSIFIED

CONTENTS

LIST OF ILLUSTRATIONS iii

I INTRODUCTION 1

II MODELING 2

A. Fourier-Transform Method 2

1. Fields Above an Imperfectly Conducting Half Space 2

2. Fields Above a Perfectly Conducting Half Space. . . 8

B. Image Method 10

1. Model 10
2. Induced Voltage 13
3. An Example of Using a Sensor Array to Determine Proximity 14

C. Reciprocity Integral 16

III EVALUATION OF INDUCTIVE ARRAY FOR NEAR-FIELD EDGE TRACKING AND RANGING 21

A. Edge Tracking 23
B. Ranging 28

IV SUMMARY 30

APPENDICES

A A TRANSFORMATION FROM k SPACE TO REAL SPACE 31
B PROJECT INTERACTIONS 36

REFERENCES 38

ILLUSTRATIONS

1. Rectangular Single-Turn Coil Parallel to the Surface of a Conducting Half Space 3

2. Array of Square Concentric Single-Turn Coils 15

3. Lift-Off versus Sensor-Voltage Ratio 17

4. Cases Used in Reciprocity Model for Computing Step Response 18

5. Sensor Array 22

6. Measurement System for Testing Sensor Array 24

7. Measured Discriminator Characteristics for Different Edge Rotations (Channel 1 - Channel 2) 24

8. Edge-Tracking Characteristics 26

9. Step Response of a Differential Sensor Pair 27

10. Ranging Characteristic of an Inductive Sensor Array 29

I INTRODUCTION

The objective of this research program has been to develop the theoretical models, design methodology, and technology needed for optimally applying near-field electromagentic sensor arrays to non-destructive evaluation (NDE) and robot control. This program was a collaborative effort by SRI International and Stanford University, supported by separate contracts. SRI has studied several types of electronically scanned arrays composed of inductive sensors, whereas Stanford[1] has placed emphasis on the use of capacitive sensors.

At SRI, we have found that small printed-circuit single-turn loops exhibit good sensitivity when used as sensors.[2] This technology allows us to fabricate high-resolution arrays readily. By addressing different elements in the array and suitably processing the resulting signals, we can realize different sensing functions with the same array. In particular, we have demonstrated the capability of using such arrays for edge tracking and ranging (proximity sensing).

II MODELING

An inductive sensor array located over an imperfectly conducting half-space can be modeled using the same Fourier-transform principles applied by Dodd and Deeds to model eddy-current coils.[3,4] If the sensor elements are further than a skin depth from the imperfectly conducting surface, it is also possible to use a simpler, but approximate, image model.[5,6] We have developed both types of models for rectangular coils under the assumption that the fields produced by a system of coils can be computed by superimposing the fields produced by each coil in the absence of the others.

A. Fourier-Transform Method

1. Fields Above an Imperfectly Conducting Half Space

Consider a current source like the rectangular, single-turn coil shown in Figure 1, but of arbitrary shape with a current density vector $\bar{i}(\bar{r})$. The quasi-static magnetic vector potential in free space for such a source located in a volume v' is $\bar{A}_0(\bar{r})\exp(j\omega t)$ where

$$\bar{A}_0(\bar{r}) = \frac{\mu_0}{4\pi} \int \frac{\bar{i}(\bar{r}')}{|\bar{r} - \bar{r}'|} \, dv' \tag{1}$$

and μ_0 is the magnetic permeability of free space.

If the half space along the negative z-axis in Figure 1 is filled with a homogeneous material of conductivity σ, the new quasi-static vector potential $\bar{A}(\bar{r})\exp(j\omega t)$ can be found by solving the equation

$$\nabla^2 \bar{A}(\bar{r}) = - \mu_0 \bar{i}(\bar{r}) + j\omega\mu_0\sigma\bar{A}(\bar{r}) \tag{2}$$

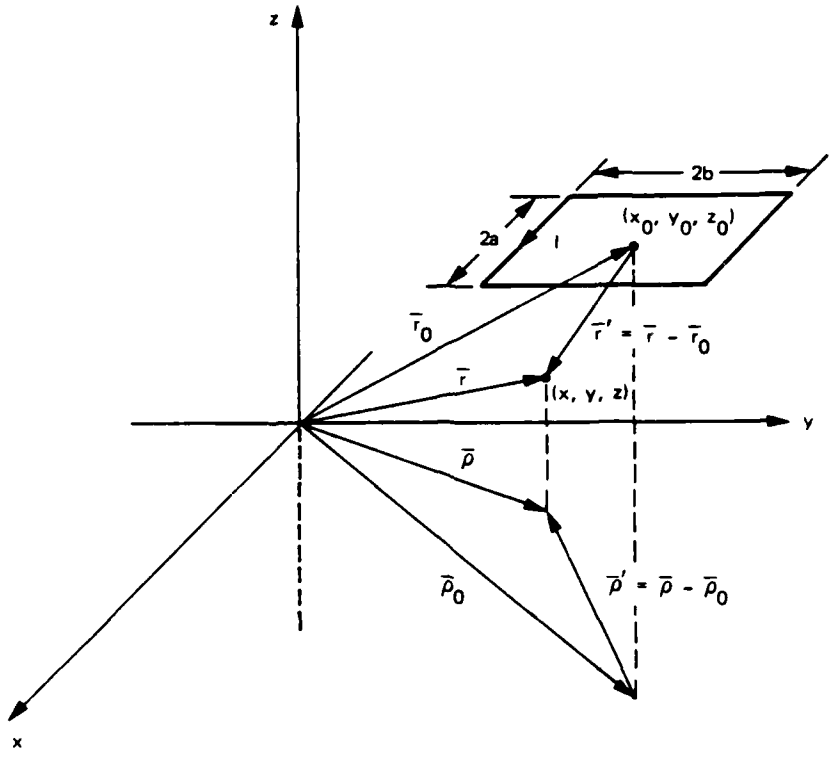

FIGURE 1 RECTANGULAR SINGLE-TURN COIL PARALLEL TO SURFACE OF CONDUCTING HALF SPACE

subject to the boundary condition that the x and y components of the electric and magnetic fields be continuous at z = 0. The solution to Eq. 2 is exponential in z. The x and y dependencies are usually found by performing a two-dimensional Fourier transform to k space, and then inverse transforming the solution to real space. The two-dimensional Fourier transform has the form:

$$a_i(\bar{k},z) = \frac{1}{2\pi}\int A_i(\bar{\rho},z)\, e^{-j\bar{k}\cdot\bar{\rho}}\, d^2\rho \quad , \quad i = x,y \tag{3}$$

where $\bar{\rho}$ and $\bar{k}$ are the vector components of the position vector $\bar{r}$ and the wave vector in the xy plane, respectively (see Figure 1).

From Eq. 2, the following equations for a_i are obtained. For $z \geq 0$:

$$-k^2 a_i^{>} + \frac{\partial^2 a_i^{>}}{\partial z^2} = -\frac{\mu_0}{2\pi} \int i_i(\bar{\rho},z)\ e^{-j\bar{k}\cdot\bar{\rho}}\ d^2\rho \quad , \tag{4}$$

and for $z \leq 0$:

$$-k^2 a_i^{<} + \frac{\partial^2 a_i^{<}}{\partial z^2} - j\omega\mu_0 a_i^{<} = 0 \quad . \tag{5}$$

Following Beissner and Sablik[4], the solution to Eq. 4 can be written as:

$$a_i^{>}(\bar{k},z) = a_i^0(\bar{k},z) + \beta_i(\bar{k})e^{-kz} \quad , \tag{6}$$

and for Eq. 5:

$$a_i^{<}(\bar{k},z) = \gamma_i(\bar{k})e^{\lambda z} \quad . \tag{7}$$

In these equations

$$\lambda = \sqrt{k^2 + j\omega\mu_0\sigma} \quad , \ k = |\bar{k}| \tag{8}$$

and

$$a_i^0(\bar{k},z) = \frac{\mu_0}{4\pi k} \int i_i(\bar{\rho}',z')e^{-j\bar{k}\cdot\bar{\rho}'-k|z-z'|}\ dv' \tag{9}$$

where $a_i^0(\bar{k},z)$ is obtained from a two-dimensional Fourier transform of $\bar{A}_0(\bar{r})$ given in Eq. 1.

The unknown coefficients $\beta_i(\bar{k})$ and $\gamma_i(\bar{k})$ are found by matching tangential components of the electric and magnetic fields at the conducting surface $z = 0$. From this condition, Beissner and Sablik derived the following expression for the magnetic vector potential in the conductor:

$$A_i^<(\bar{\rho},z) = \frac{1}{2\pi} \int a_i^<(\bar{k},z)\ e^{j\bar{k}\cdot\bar{\rho}}\ d^2k \tag{10}$$

where

$$a_x^<(\bar{k},z) = 2\ \frac{k_y}{k(\lambda + k)} \left[k_y a_x^0(\bar{k},0) - k_x a_y^0(\bar{k},0)\right] \quad , \tag{11}$$

$$a_y^<(\bar{k},z) = -\ \frac{k_x}{k_y}\ a_x^<(\bar{k},z) \quad , \tag{12}$$

and

$$a_z^<(\bar{k},z) = 0 \quad . \tag{13}$$

However, in analyzing an electromagnetic sensor array, the electric and magnetic fields above the conducting surface are of particular interest. These fields can be determined by matching the expression for $a_i^>(\bar{k},z)$ (Eq. 6) and $a_i^<(\bar{k},z)$ (Eqs. 11-13) at $z = 0$. The resulting equations are

$$a_x^>(\bar{k},z) = a_x^0(\bar{k},0)\left(e^{kz} + \frac{k-\lambda}{k+\lambda}\ e^{-kz}\right) \quad , \tag{14}$$

$$a_y^>(\bar{k},z) = -\ \frac{k_x}{k_y}\ a_x^>(\bar{k},z) \quad , \tag{15}$$

and

$$a_z^>(\bar{k},z) = 0 \quad . \tag{16}$$

The electric and magnetic fields above the conducting surface, $\bar{E}^>$ and $\bar{H}^>$, are then determined from

$$\vec{E}(\bar{r}) = - j\omega \vec{A}(\bar{\rho},z) \tag{17}$$

and

$$\vec{H}(\bar{r}) = \frac{1}{\mu_0} \nabla \times \vec{A}(\bar{\rho},z) \tag{18}$$

where

$$A_i(\bar{\rho},z) = \frac{1}{2\pi} \int a_i(\bar{k},z) e^{j\bar{k}\cdot\bar{\rho}} \, d^2k \quad . \tag{19}$$

Now consider the special case shown in Figure 1, where we have a single-turn, infinitely thin, rectangular coil carrying a current I in a plane parallel to the surface z = 0. To find the electric and magnetic field for this configuration, we must find the current density i_i so that $a_i^0(\bar{k},z)$ can be calculated from Eq. 9. These current-density components can be written as

$$i_x(x,y,z) = I\delta(z-z_0)\left(\delta\left[y-(y_0-a)\right] - \delta\left[y-(y_0+a)\right]\right) \text{rect}\left(\frac{x-x_0}{2a}\right) \quad , \tag{20}$$

$$i_y(x,y,z) = I\delta(z-z_0)\left(\delta\left[x-(x_0-b)\right] - \delta\left[x-(x_0+b)\right]\right) \text{rect}\left(\frac{y-y_0}{2b}\right) \quad , \tag{21}$$

and

$$i_z(x,y,z) = 0 \quad . \tag{22}$$

Inserting these expressions into Eq. 9 we obtain

$$a_x^0(\bar{k},z) = j \frac{\mu_0 I}{\pi k k_x} \sin(k_x a) \sin(k_y b) e^{-j\bar{k}\cdot\bar{\rho}_0} e^{-k|z-z_0|} \quad , \tag{23}$$

$$a_y^0(\bar{k},z) = - \frac{k_x}{k_y} a_x^0(\bar{k},z) \quad , \tag{24}$$

and

$$a_z^0(\bar{k},z) = 0 \quad . \tag{25}$$

Combining Eqs. 23 and 14 and inserting the resulting $a_i^>(\bar{k},z)$ into the integral of Eq. 19 results in very complex integrals because of the factor $(k-\lambda)/(k+\lambda)$ that occurs in the expressions for $a_i^>(\bar{k},z)$. This factor also appears in the image theory for this problem[5], where it is shown that it can be approximated by

$$\frac{k-\lambda}{k+\lambda} \simeq - \exp(-kd) \tag{26}$$

when the receiver (sensor array) is more than a skin depth away from the conductor surface. The factor d in this expression is related to the skin depth

$$\delta = \sqrt{2/(\omega\mu_0\sigma)} \tag{27}$$

by the relation

$$d = (1-j)\delta \quad . \tag{28}$$

Using the approximation given by Eq. 26 we obtain

$$a_x^>(\bar{k},z) = 2a_x^0(\bar{k},0) \exp(-kd/2) \sinh[k(z + \tfrac{d}{2})] \quad . \tag{29}$$

For a perfect conductor ($\sigma \to \infty$), d = 0 and Eq. 29 simplifies to

$$a_x^>(\bar{k},z) = 2a_x^0(\bar{k},0) \sinh(kz) \quad . \tag{30}$$

Comparing Eqs. 29 and 30, we note that, if the factor exp(-kd/2) is included in the expression for $a_x^0(\bar{k},0)$ in Eq. 23, the approximate solution for the case of a conducting half-space with finite conductivity is the same as that for a perfectly conducting half-space, except that z is replaced by z + d/2. This result will be discussed further in a subsequent section on image theory.

2. Fields Above a Perfectly Conducting Half Space

When $a_x^>(\bar{k},z)$ in Eq. 30 for a perfect conductor is used in Eq. 19, the following expressions for the electric and magnetic fields are obtained from Eqs. 17 and 18 for $z \geq 0$:

$$E_x(x,y,z) = -\frac{j\omega}{\pi}\int \sinh(kz)\ a_x^0(\bar{k},0)e^{j\bar{k}\cdot\bar{\rho}}\ d^2k \tag{31}$$

$$E_y(x,y,z) = \frac{j\omega}{\pi}\int \frac{k_x}{k_y}\sinh(kz)\ a_x^0(\bar{k},0)e^{j\bar{k}\cdot\bar{\rho}}\ d^2k \tag{32}$$

$$E_z(x,y,z) = 0 \tag{33}$$

$$H_x(x,y,z) = -\frac{1}{\mu_0\pi}\int \frac{k_x k}{k_y}\cosh(kz)\ a_x^0(\bar{k},0)e^{j\bar{k}\cdot\bar{\rho}}\ d^2k \tag{34}$$

$$H_y(x,y,z) = \frac{1}{\mu_0\pi}\int k\cosh(kz)\ a_x^0(\bar{k},0)e^{j\bar{k}\cdot\bar{\rho}}\ d^2k \tag{35}$$

$$H_z(x,y,z) = 0 \tag{36}$$

The integrations appearing in these equations are evaluated using sine and cosine tranforms that are discussed in Appendix A. The results are:

$$E_x = j \frac{\omega\mu_0 I}{4\pi} \Big[F_x(-z,\rho_x',-\rho_y') + F_x(-z,-\rho_x',-\rho_y') +$$

$$F_x(z,\rho_x',\rho_y') + F_x(z,-\rho_x',\rho_y') -$$

$$\Big(F_x(-z,\rho_x',\rho_y') + F_x(-z,-\rho_x',\rho_y') +$$

$$F_x(z,\rho_x',-\rho_y') + F_x(z,-\rho_x',-\rho_y') \Big) \Big] \qquad (37)$$

where

$$F_x(\pm z,\pm\rho_x',\pm\rho_y') = \ell n \left(\frac{a \pm \rho_x' + \sqrt{(a \pm \rho_x')^2 + (b \pm \rho_y')^2 + (z_0 \pm z)^2}}{\sqrt{(b \pm \rho_y')^2 + (z_0 \pm z)^2}} \right) . \qquad (38)$$

and ρ_x' and ρ_y' are the x and y components of the vector $\bar{\rho}-\bar{\rho}_0$. E_x consists of eight terms containing all possible combinations of the variables $\pm z$, $\pm\rho_x'$, and $\pm\rho_y'$. E_y is obtained by changing the sign of the right side of Eq. 37 and making the following substitutions in Eqs. 37 and 38;

$$a \rightarrow b,\ b \rightarrow a,\ \rho_x' \rightarrow \rho_y',\ \text{and}\ \rho_y' \rightarrow \rho_x' \quad . \qquad (39)$$

Finally,

$$E_z = 0 \quad . \qquad (40)$$

Similarly, H_y can be written as

$$H_y = \frac{I}{4\pi} \left[\sum^{sign} G_y(\pm z,\pm\rho_x',-\rho_y') - \sum^{sign} G_y(\pm z,\pm\rho_x',\rho_y') \right] \qquad (41)$$

where

$$G_y(\pm z, \pm\rho_x', \pm\rho_y') = \frac{(z_0 \pm z)\,(a \pm \rho_x')}{\left[(b \pm \rho_y')^2 + (z_0 \pm z)^2\right]\sqrt{(a \pm \rho_x')^2+(b \pm \rho_y')^2+(z_0 \pm z)^2}} \quad . \tag{42}$$

The symbol $\sum^{sign}$ in Eq. 41 denotes the sum over all possible sign combinations of the variables in G_y so that each sum appearing in Eq. 41 consists of four terms. H_x is obtained by making the substitution shown in Eq. 39 in Eqs. 41 and 42. Finally,

$$H_z = 0 \quad . \tag{43}$$

B. Image Method

1. Model

The Fourier-transform method used in the previous section is quite powerful and provides an exact solution to the problem of calculating the fields generated by a coil over an imperfectly conducting half space. However, this method leads to integrals that must be evaluated over infinite domains in the complex plane, which may be difficult to do. Therefore, for such half-space problems, it is usually simpler to use image theory. Of course, image theory is only exact for perfect conductors, but, as has been mentioned in Section II-A-1, it can be extended to apply to imperfect conductors in an approximate, but simple, way.

To develop the image theory for a rectangular coil lying in a plane parallel to a conducting half space, we again refer to Figure 1. The current, I, flowing in the coil produces a vector potential, $\bar{A}^+$, in the absence of the half space given by

$$A_x^+(\bar{r}) = \frac{\mu_0 I}{4\pi} \int_{x_0-a}^{x_0+a} \left\{ \frac{e^{-jkR_1}}{R_1} - \frac{e^{-jkR_3}}{R_3} \right\} dx' \qquad (44a)$$

and

$$A_y^+(\bar{r}) = \frac{\mu_0 I}{4\pi} \int_{y_0-b}^{y_0+b} \left\{ \frac{e^{-jkR_2}}{R_2} - \frac{e^{-jkR_4}}{R_4} \right\} dy' \qquad (44b)$$

where

$$R_1 = \sqrt{(x - x')^2 + (r_y' + b)^2 + (z - z_0)^2} \quad , \qquad (45a)$$

$$R_2 = \sqrt{(r_x' - a)^2 + (y - y')^2 + (z - z_0)^2} \quad , \qquad (45b)$$

$$R_3 = \sqrt{(x - x')^2 + (r_y' - b)^2 + (z - z_0)^2} \quad , \qquad (45c)$$

and

$$R_4 = \sqrt{(r_x' + a)^2 + (y - y')^2 + (z - z_0)^2} \quad . \qquad (45d)$$

The quantities r_x', r_y' in Eq. (45) are the x and y components of $\bar{r}'$. The integrals in Eqs. 44 are easily evaluated under the quasistatic approximation $kR \ll 1$. The results are

$$A_x^+(\bar{r}) = \frac{\mu_0 I}{4\pi} \ln \left\{ \frac{\left[R(\bar{r}';-a,b) - (r_x'-a)\right]\left[R(\bar{r}';a,-b) - (r_x'+a)\right]}{\left[R(\bar{r}';a,b) - (r_x'+a)\right]\left[R(\bar{r}';-a,-b) - (r_x'-a)\right]} \right\} \tag{46a}$$

and

$$A_y^+(\bar{r}) = \frac{\mu_0 I}{4\pi} \ln \left\{ \frac{\left[R(\bar{r}';-a,-b) - (r_y'-b)\right]\left[R(\bar{r}';a,b) - (r_y'+b)\right]}{\left[R(\bar{r}';-a,b) - (r_y'+b)\right]\left[R(\bar{r}';a,-b) - (r_y'-b)\right]} \right\} \tag{46b}$$

where

$$R(\bar{r}';\pm a,\pm b) = \sqrt{(r_x' \pm a)^2 + (r_y' \pm b)^2 + (z - z_0)^2} \quad . \tag{47}$$

For a perfectly conducting halfspace, the vector potential, $\bar{A}^-$, due to the image current can be obtained from Eq. 46 by letting $I \rightarrow -I$ and $z_0 \rightarrow -z_0$. The total vector potential is just the sum of the two parts, viz.,

$$\bar{A}(\bar{r}) = \bar{A}^+(\bar{r}) + \bar{A}^-(\bar{r}) \quad . \tag{48}$$

Finally, the electromagnetic fields can be found from the vector potential by using the relations

$$\bar{E}(\bar{r}) = -j\omega\bar{A}(\bar{r}) \quad . \tag{49a}$$

and

$$\bar{H}(\bar{r}) = (1/\mu_0)\ \nabla \times \bar{A}(\bar{r}) \quad . \tag{49b}$$

It can be shown that these equations are identical to those obtained in Section II-A-2 using the Fourier-transform method.

For an imperfectly conducting half space, it has been shown[5] that the fields above the half space can be determined to good approximation by placing the image at a complex depth $-(z_0+d)$ where d is given by Eq. 28. Similarly, for an imperfectly conducting layer of thickness t on top of an imperfectly conducting half space, an approximate image model can be obtained by using[6]

$$d = (1 - j)\delta Q \tag{50}$$

where

$$Q = \frac{1 - e^{-4t/(1-j)\delta}}{1 + e^{-4t/(1-j)\delta}} \quad . \tag{51}$$

Although approximate, these formulas allow us to model imperfect half-space and layered half-space problems in a very simple way.

2. Induced Voltage

To compute the voltage induced in different sensor coils by a separate exciting (driver) coil, we use Faraday's Law

$$V_{Sense} = -j\omega \int_S (\nabla \times \bar{A}) \cdot d\bar{S} \tag{52}$$

where S is the surface area enclosed by the coil. Alternatively, we can use Stoke's Theorem to write this equation as a line integral along the conductor that defines the coil, viz.,

$$V_{Sense} = -j\omega \oint \bar{A} \cdot d\bar{\ell} \quad . \tag{53}$$

This latter equation is simpler to evaluate since it uses $\bar{A}$ directly. Note that throughout our development, we assume that wire in the coil has very small cross sectional dimensions so that the current in the coil can be represented by a delta function in this cross section plane.

3. An Example of Using a Sensor Array to Determine Proximity

The response of an inductive sensor array depends on its proximity to (lift-off from) a nearby conducting half-space. Thus, it is of interest to examine the possibility of inverting the array response to provide a quantitative measure of the distance of the array from the half space.

As a simple example, consider the array of concentric rectangular coils shown in Figure 2. The outermost coil is an exciting coil, and the inner coil is a sensor. The coil axes are assumed to be perpendicular to a perfectly conducting half space, and the coils are located at a distance z_0 above the half space (if the half space is imperfectly conducting, the approximations discussed in Section II-B-1 can be used in analyzing this problem). The problem is to determine z_0, given the array response.

From Eq. 53, the voltage induced in the inner coil by the outer coil is

$$V_{Sense} = -j\omega \left\{ \int_{-\alpha a}^{\alpha a} \left[A_x^+(x', -\alpha a, z_0) - A_x^+(x', \alpha a, z_0) \right] dx' \right.$$

$$+ \int_{-\alpha a}^{\alpha a} \left[A_y^+(\alpha a, y', z_0) - A_y^+(-\alpha a, y', z_0) \right] dy'$$

$$\left. + \text{image terms} \right\} \quad . \tag{54}$$

The vector potential produced by the exciting coil is given by Eq. 46. Substituting the values of A_x^+ and A_y^+ of Eq. 46 into Eq. 54 results in a nonstandard integral of the form

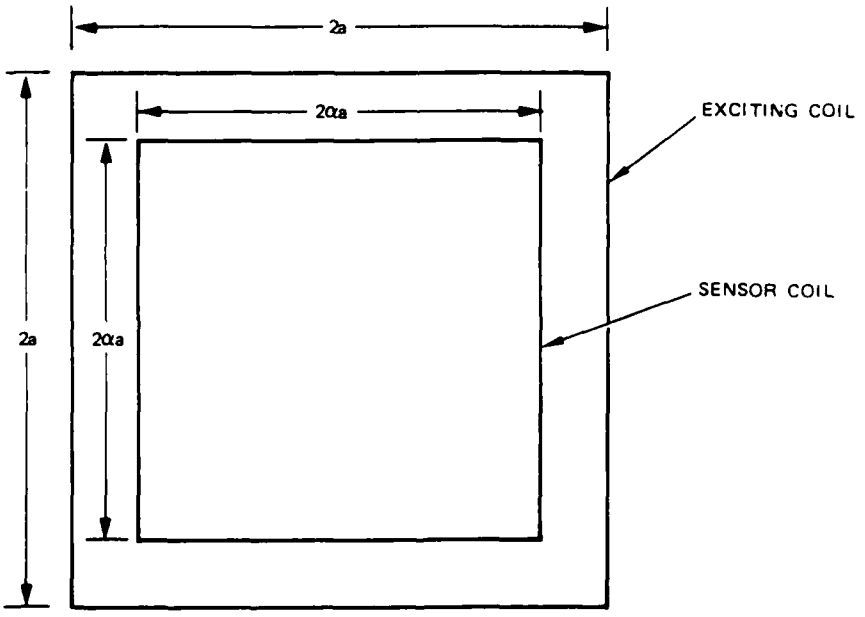

FIGURE 2 ARRAY OF SQUARE CONCENTRIC SINGLE-TURN COILS

$$\int \ell n \left[\sqrt{X^2 + Y^2} - X \right] dX \quad . \tag{55}$$

This integration has been carried out symbolically using a computer program called MAXIMA, and the result is

$$\sqrt{X^2 + Y^2} + Y + X \ell n \left[\sqrt{X^2 + Y^2} - X \right] \quad . \tag{56}$$

To avoid a need for system calibration, we assume there are two sense coils, one inside the other, and calculate the ratio of the voltages induced in them by the exciting coil. For this calculation, we assume that both the source and detector impedances are large enough so that back reaction of the sense coils on the exciting coil is negligible, as is interaction between the sense coils.

The normalized lift-off distance, $\tilde{z}_0 = z_0/a$ is shown in Figure 3 plotted versus the voltage ratio computed using Eq. 54. The scale of the inner sense coil was taken to be $\alpha = 0.2$, while the size of the outer sense coil was allowed to vary through the values of α shown in the figure. We see that, the larger the outer sense coil, the better the resolution for determing $\tilde{z}_0$. For $\alpha = 0.8$, the lift-off, z_0, can be determined most accurately for values of z_0 between about 0.03a and 0.3a.

C. Reciprocity Integral

So far, our modeling has been concerned with a relatively simple geometry, namely, a half space. It is also important to model situations where the sensor array is scanned parallel to the surface of the half space in order to detect or track discontinuities in this half space. The reciprocity method described by Auld[7] is useful for this purpose. We illustrate this method for the case where there is a step in the surface of a perfectly conducting half space.

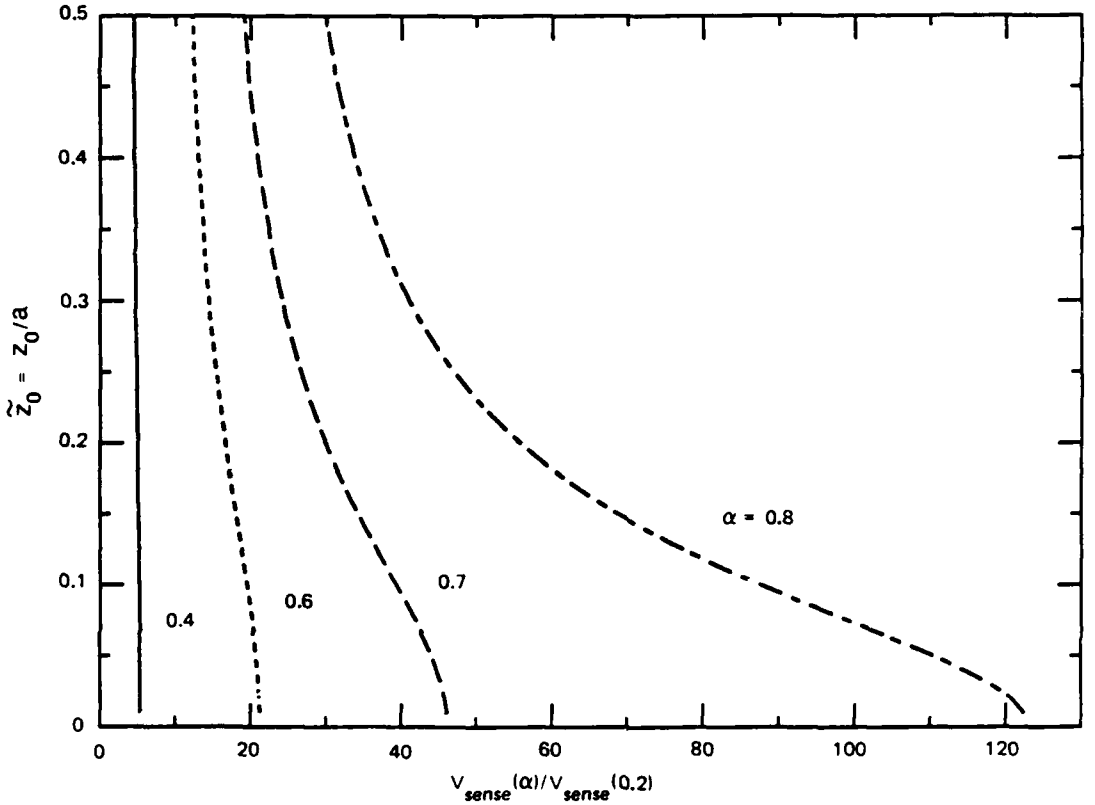

FIGURE 3 LIFT-OFF vs SENSOR-VOLTAGE RATIO

To compute the result of scanning a perfectly balanced differential sensor pair across a small step in a conducting plane requires that the E and H fields produced by the two coil configurations shown in Figure 4 be computed. Using these fields, the step response of the sensor pair can then be computed by evaluating the following reciprocity integral for each sensor-pair position (x_0, y_0, z_0):

$$\frac{V_2^{(1)}}{V_a} = -\frac{Z_b}{V_a V_b} \int\int \left\{ \bar{E}^{(1)} \times \bar{H}^{(2)} - \bar{E}^{(2)} \times \bar{H}^{(1)} \right\} \cdot \hat{a}_z \, dxdy \quad . \qquad (57)$$

In this equation, the superscripts refer to the two cases defined in Figure 4 and $\hat{a}_z$ is a unit vector in the z direction. The integral is evaluated on the plane $z = 0$.

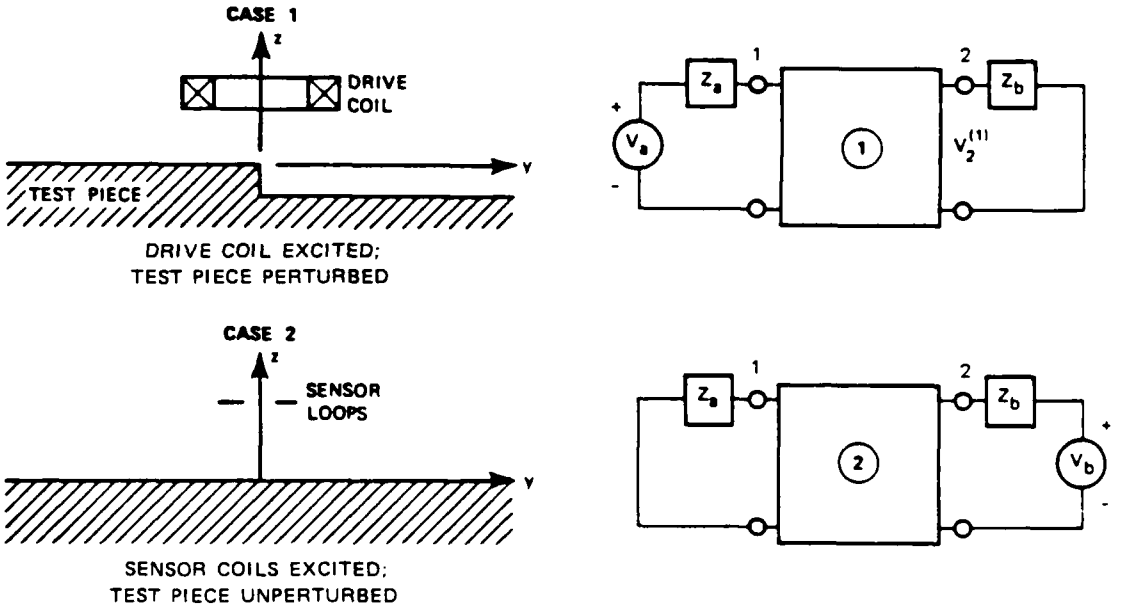

FIGURE 4 CASES USED IN RECIPROCITY MODEL FOR COMPUTING STEP RESPONSE

For a perfect conductor, Eq. 57 can be simplified by making use of the vector identity

$$\left(\bar{E} \times \bar{H}\right) \cdot \hat{a}_z = \bar{E} \cdot \left(\bar{H} \times \hat{a}_z\right) = \bar{H} \cdot \left(\hat{a}_z \times \bar{E}\right) \quad . \tag{58}$$

Since $\hat{a}_z \times \bar{E}$ is proportional to the component of $\bar{E}$ tangential to the x-y plane, $(\bar{E}^{(2)} \times \bar{H}^{(1)}) \cdot \hat{a}_z = 0$ everywhere on the plane $z = 0$. Similarly, $(\bar{E}^{(1)} \times \bar{H}^{(2)}) \cdot \hat{a}_z$ also equals zero on this plane for $y < 0$. Hence, Eq. 57 reduces to

$$\frac{V_2^{(1)}}{V_a} = - \frac{Z_b}{V_a V_b} \int_{-\infty}^{\infty} dx \int_{0}^{\infty} \left[E_x^{(1)} H_y^{(2)} - E_y^{(1)} H_x^{(2)}\right] \, dy \quad . \tag{59}$$

This formula is exact. However, there are no analytic formulas for calculating the electric fields in case 1, and approximations are often used. The approximation we have used to compute the results given in Section III-A is to assume that there is no step in the conducting half space, but, rather that the half space is displaced downward everywhere from $z = 0$ by the step height. This should be a good approximation if the step height is small compared to the radius of the drive coil used in case 1.

Similar simplifications to Eq. 57 can also be achieved when the stepped half space is imperfectly conducting. For example, if we assume that the tangential fields $\bar{E}_t$ and $\bar{H}_t$ are approximately related by a scalar surface impedance[8], Z_s, viz.,

$$\hat{a}_z \times \bar{E} \simeq Z_s \bar{H}_t \quad , \tag{60}$$

then

$$\left[\bar{E}^{(1)} \times \bar{H}^{(2)} - \bar{E}^{(2)} \times \bar{H}^{(1)}\right] \cdot \hat{a}_z \simeq \Delta Z_s \bar{H}_t^{(1)} \cdot \bar{H}_t^{(2)} \qquad (61)$$

where

$$\Delta Z_s = Z_s^{(1)} - Z_s^{(2)} \quad . \qquad (62)$$

If Z_s is known at the conducting surface, then $Z_s^{(1)}$ on $z = 0$ for $y > 0$ can be estimated using the well-known transmission-line impedance-transformation formula. Although, in general, the ratio of E_t/H_t varies with position on the surface under a coil[9], use of a surface impedance in this manner should be a good approximation for good conductors.

III EVALUATION OF INDUCTIVE ARRAYS FOR NEAR-FIELD EDGE TRACKING AND RANGING

In previous work on this project, SRI demonstrated that small single-turn printed loops can be used as sensors with sufficient sensitivity to be useful in NDE and robotics and that printed-circuit techniques facilitate the fabrication of arrays of small loops to provide electronic scanning with high spatial resolution. To further evaluate this capability, we have built such an array and have evaluated its use for closed-loop edge tracking and for ranging (proximity sensing).

The sensor elements used in this work consisted of single-turn rectangular loops with inner dimensions of 0.030 by 0.050 in. The loops are printed on circuit boards using standard techniques, and the width of each printed line is 0.005 in. A typical arrangement of two rows, each with four loops, is shown in Figure 5(a). The center-to-center spacing of adjacent loops in a row is 0.070 in., and the distance between adjacent printed lines of two neighboring loops is 0.010 in. To complete the probe system, a magnetic drive field is provided by a 30-turn, 0.5-in. square coil (not shown), with its axis perpendicular to the circuit board. This arrangement results in a two-port probe (called a reflection probe in eddy-current testing); the drive coil is the probe's input, and the sensor loop(s) is (are) its output.

To detect an edge or groove in a metal surface, it is best to minimize lift-off sensitivity by connecting an adjacent pair of sensor loops differentially as shown in Figure 5(b). For the edge-tracking experiment described below, we used the signals from the two staggered pairs of sensor loops designated as Channels 1 and 2 in Figure 5(a). On the other hand, for ranging (lift-off) measurements, we used the signals obtained separately from each of the four loops in a row.

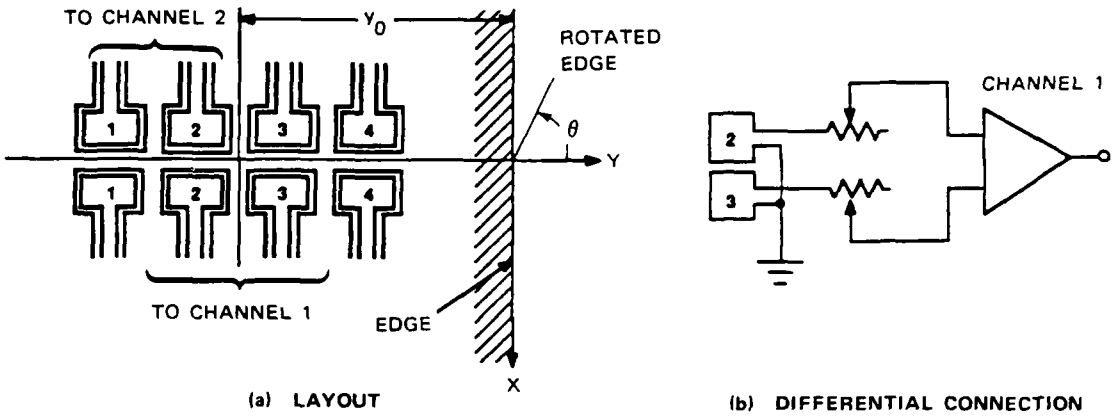

FIGURE 5 SENSOR ARRAY

Addressing the loops in pairs or individually was accomplished using a thin-film, four-channel read/write amplifier made by Silicon Systems (SSI 520). Channel selection in this amplifier is controlled by the data acquisition computer. The two 1-kΩ potentiometers shown in Figure 5(b) are used to balance the inputs from the two loops (for the differential connection) and to provide the proper input impedance for the amplifier. For single-loop measurements, the resistance of each potentiometer was set to 100 Ω.

A block diagram of the measurement system used on our experiments is shown in Figure 6. The probe's drive coil is excited by a stable generator operating at 250 kHz and an available power level of 0 dBm. This drive level gives a sensor-loop voltage level of the order of 10 μV. The output from the differential amplifier is filtered by a 250-Hz crystal filter, amplified by 60 dB, and measured by a Solartron computing voltmeter (Model 7151). The level of the signal voltage measured by the voltmeter is of the order of 1 V, and the corresponding background noise

level is about 1 mV. The digital value of the voltage measured by the voltmeter is then fed to an HP1000 computer. This same computer also selects the channel to be measured, performs any required computations on the measured voltages, and using a suitable algorithmic interpretation of these voltages as a basis, controls the position of the X-Y stage.

A. Edge Tracking

Tracking an edge requires that the sensor array generate a discrimination function such that a change in the sign of the measured voltage indicates the proximity of an edge. Such a discrimination function can be generated by subtracting the outputs of Channels 1 and 2 shown in Figure 5(a). Three discrimination functions measured using our array are shown in Figure 7. These functions were obtained by scanning the array over a 0.25-in.-deep, 0.5-in.-wide slot in a flat aluminum plate (only the response from one edge of the slot is shown).

The discriminator voltage is plotted in Figure 7 as a function of the relative position of the array center, y_0, with respect to the edge. The array center was located as close as possible to the center of the drive coil. Because the two sensor pairs that make up Channels 1 and 2 are displaced assymetrically with respect to the array center, the discrimination function crosses zero when the array center is to the right of the edge (about 0.035 in. when the edge is perpendicular to the scan direction). The slope of the discrimination function depends on the relative displacement of the two sensor pairs, which is 0.070 in. The noticeable assymetry of these functions around the zero crossing is caused by the nonuniformity of the drive field, the relative setting of the potentiometers, and the influence of the other edge of the slot at large values of y_0.

As can be seen in Figure 7, the shape of the discrimination function varies with the angle θ between the scan direction and the edge. When θ

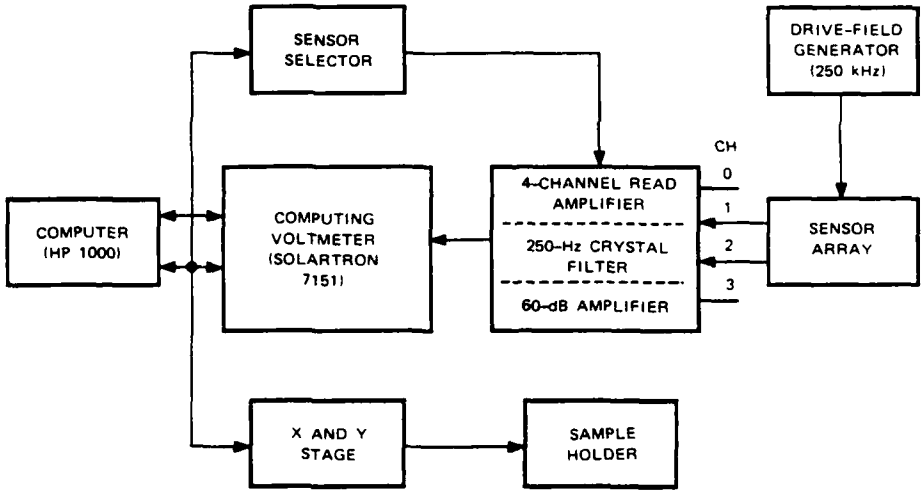

FIGURE 6 MEASUREMENT SYSTEM FOR TESTING SENSOR ARRAY

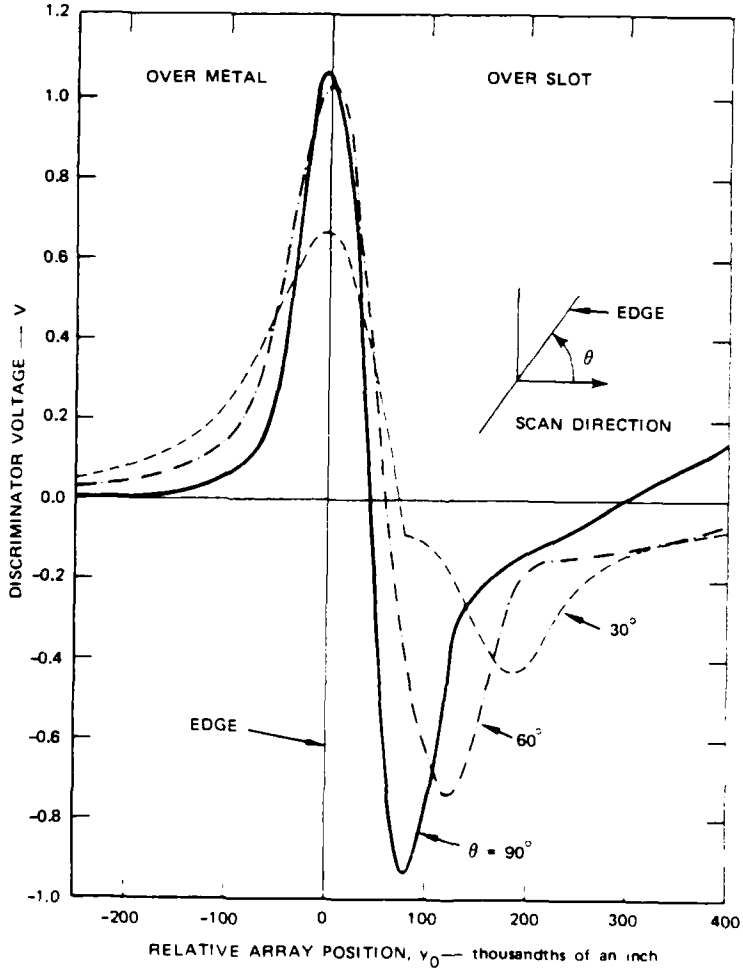

FIGURE 7 MEASURED DISCRIMINATOR CHARACTERISTICS FOR DIFFERENT EDGE ROTATIONS (CHANNEL 1 – CHANNEL 2)

decreases, the two peaks of this function move apart by an amount proportional to $1/\sin\theta$, and the peak values decrease. This kind of behavior occurs because the connections that are used in these experiments produce an array that is polarized along the rows of sensor loops.

A simple edge-tracking algorithm was programmed into the computer to demonstrate experimentally that such a sensor array can be made to follow an edge. The resulting measured edge-tracking characteristics of the system are shown in Figures 8(a) and 8(b) for edge angles of $\theta = 60°$ and 30°, respectively. These characteristics were produced as follows: the search for the edge starts with a sensor location corresponding to the left side of the zero crossing in the discrimination curve. The sensor steps along the horizontal y axis (0.010-in. steps were used in this case) until the discriminator voltage changes sign. At this point, the sensor steps in the positive x (vertical) direction. If this step increases the discriminator voltage, the scan direction is reversed; otherwise the scan continues in the same direction. The x scan continues until the discriminator voltage changes sign again. At this point, the probe steps one step in the y direction and the cycle is repeated.

The staircase-shaped curves shown in Figure 8 depict the endpoints of the probe's movement; any backtracking that is required to reach these endpoints is not explicitly shown. There was no backtracking in the step sequence depicted in Figure 8(a). For this case, the probe stepped vertically along the discriminator curve from A→A'→B, then horizontally from B→C, then vertically from C→D, and so forth. On the other hand, the step sequence shown in Figure 8(b) did involve backtracking. One vertical step was required to go from A→B. Then one horizontal step moved the operating point along the discriminator curve from B→C with no change in sign. However, the next vertical step moves one from C→C'', which is in the wrong direction. The probe, therefore, reverses direction, moving the operating point from C'→C''--because of backlash, C'' and C do not coincide. Because no change in sign occurred as a result of this last step, another vertical step is taken, which results in the move C''→D.

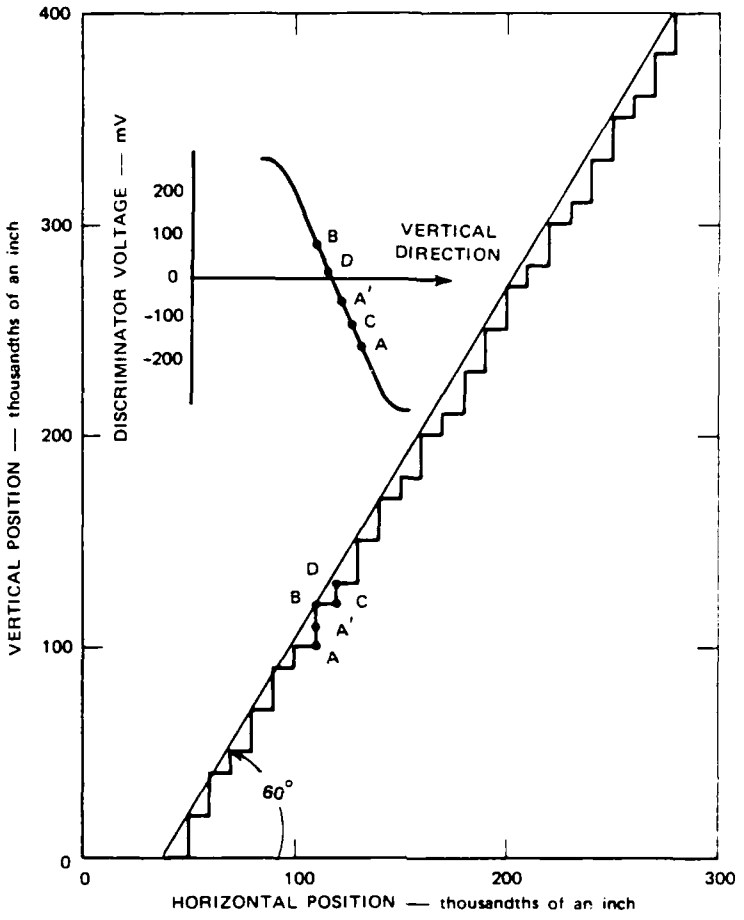

(a) 60° EDGE ANGLE

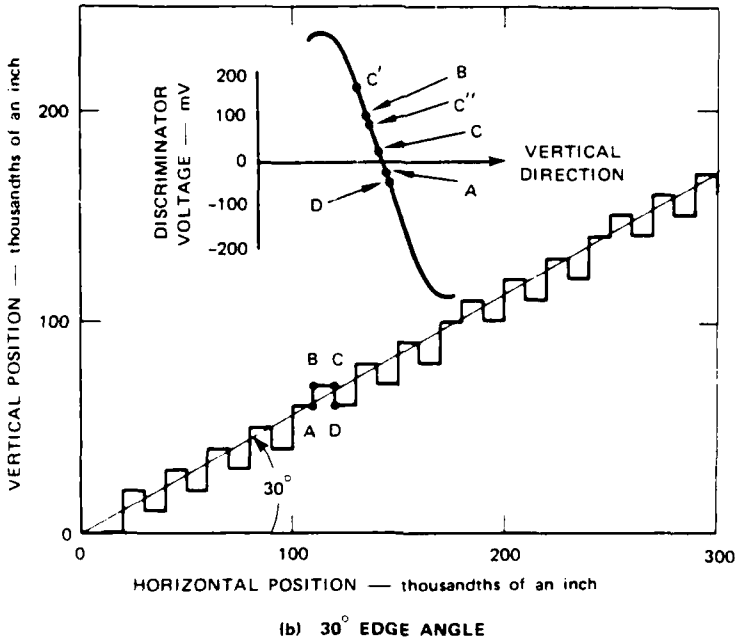

(b) 30° EDGE ANGLE

FIGURE 8 EDGE-TRACKING CHARACTERISTICS (0.010-in. STEPS)

Both of these characteristics were generated in real time, thereby demonstrating the feasibility of tracking an edge using such a sensor array. No significant difference in tracking was noted between the 30° and 60° cases, even though the respective discrimination functions are different. Similar tracking characteristics were also generated using 0.002-in. steps, thereby demonstrating that excellent signal-to-noise ratios were obtained. Finally, the straight lines drawn in Figure 8 are for angle-reference purposes only; they do not represent the position of the edge. Determining the edge position with respect to the track requires additional calibration of the probe.

In addition to this experimental work, the step response of the array was modeled using the approximate theory described in Sectio II-C. The computed differential response of a pair of rectangular sensor loops to a 0.004-in.-step in an alluminum plate is compared with the corresponding experimental results in Figure 9. The array position has been normalized to one half the inner dimension of the drive coil. In this case, the peak response occurs when the sensor pair is located symmetrically over the edge of the step. Because the measurement is uncalibrated, the

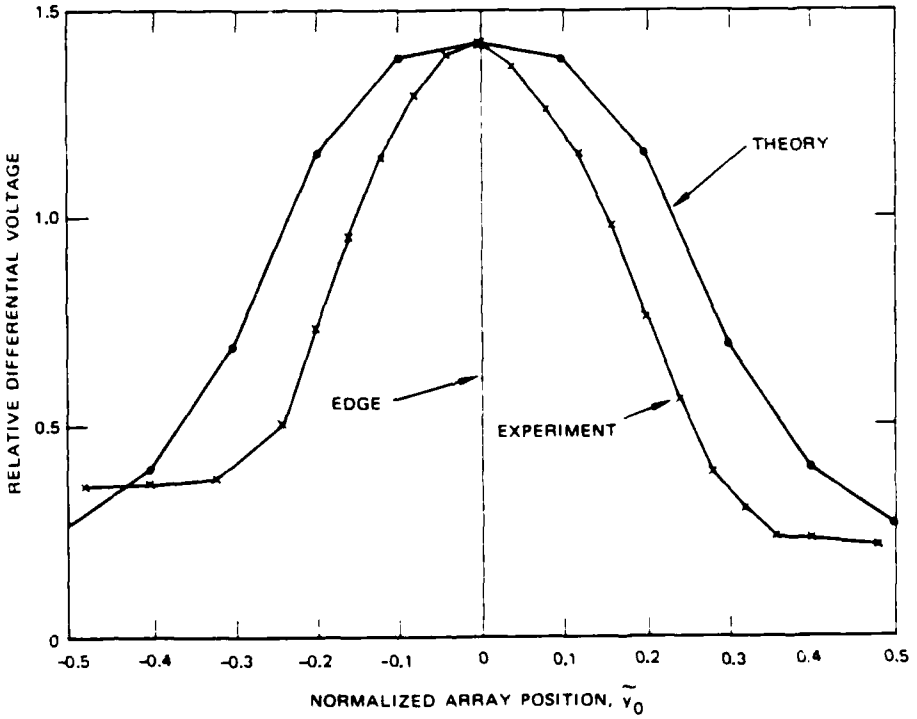

FIGURE 9 STEP RESPONSE OF A DIFFERENTIAL SENSOR PAIR

experimental and theoretical curves were arbitrarily normalized to make the peak values equal for this comparison. We see that the theoretical response curve is noticeably wider than the measured curve. Determining the reason for this discrepancy will require further study.

B. Ranging

Experiments were also performed to demonstrate that the distance from the sensor array to the workpiece surface can be determined from the measured outputs of the array elements without moving the array. This is different from the case of a single absolute eddy-current probe, in which the distance of the probe from the underlying surface can only be determined if the probe output is measured at several different distances above the surface. Our ability to determine range, using a stationary array, is based on the fact that different elements in the array sample the spatial-frequency content of the drive field differently.

To eliminate the effect of the measurement-system transfer function in determining range, we measured the ratio of two voltages sensed by different elements in the array as a function of lift-off distance. For maximum range resolution, the elements used to generate this ratio should be located in regions where the drive field differs as much as possible with respect to spatial variation. We used one row of four loops and formed the desired ratio by dividing the sum of the voltages sensed by the two loops furthest from the center of the drive coil, by the sum of the voltages sensed by the two loops closest to the drive coil's center. The resulting measured ranging characteristic is shown in Figure 10, in which the lift-off distance (normalized to one half of the inner dimension of the drive coil) is plotted versus voltage ratio. It is seen that a 10-percent change in voltage ratio corresponds to about a 50-percent change in lift-off distance for a normalized lift off of less than about 0.3. This sensitivity is usable, but not large. We expect that a different array geometry might improve this sensitivity.

Using the image theory discussed in Section II-B, we computed the theoretical ranging characteristic for this array and also plotted it in

Figure 10. The shapes of the theoretical and experimental curves are similar, but they exhibit significant quantitative differences. We attribute these differences to the fact that the model ignored the conducting tape that was used to shield the sensor leads on the circuit board in the vicinity of the loops.

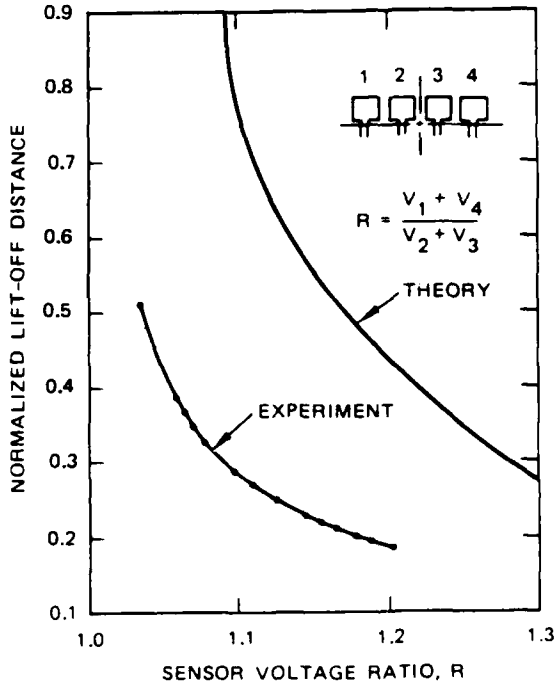

FIGURE 10 RANGING CHARACTERISTIC OF AN INDUCTIVE SENSOR ARRAY

IV SUMMARY

It has been demonstrated that an array of small single-turn printed sensor loops can be used for high-resolution edge tracking. Also, with proper calibration, absolute range can be determined from a ratio of sensor voltages without moving the array. Other possible uses for such an array are in material characterization and two-dimensional eddy-current imaging. Finally, an approximate model for computing the array response has been developed, but further work to improve its accuracy is required.

APPENDIX A

TRANSFORMATION FROM k SPACE TO REAL SPACE

Transformation of the electric and magnetic fields given by Eqs. 31-36 from k space to real space is obtained by transforming E_x and H_y, and noting that E_y and H_x can be obtained by making a simple substitution in the expressions for E_x and H_y and a sign change in E_x.

Using Eqs. 23 and 31, E_x can be written as,

$$E_x = \frac{\omega\mu_0 I}{\pi^2} \int_{-\infty}^{\infty} \int_{-\infty}^{\infty} \frac{1}{k\ k_x} \sinh(kz)\ \sin(k_x a)\ \sin(k_y b) e^{j\bar{k}\cdot(\bar{\rho}-\bar{\rho}_0)} e^{-kz_0}\ dk_x\ dk_y \quad . \tag{A1}$$

If we write this equation as

$$E_x = \frac{\omega\mu_0\ I}{\pi^2} \int_{-\infty}^{\infty} \int_{-\infty}^{\infty} f(k_x, k_y) e^{j\bar{k}\cdot(\bar{\rho}-\bar{\rho}_0)}\ dk_x\ dk_y \tag{A2}$$

and use

$$k = \sqrt{k_x^2 + k_y^2} \quad , \tag{A3}$$

we note that $f(k_x, k_y)$ is even in k_x and odd in k_y. Hence, the only part of $e^{j\bar{k}\cdot(\bar{\rho}-\bar{\rho}_0)}$ expressed in terms of sine and cosine functions that contributes to the integral is $j\cos(k_x\rho_x')\sin(k_y\rho_y')$ where ρ_x' and ρ_y' are the x and y components of the vector $\bar{\rho}-\bar{\rho}_0$. Eq. A1 can therefore be rewritten as

$$E_x = j\frac{\omega\mu_0 I}{\pi^2}\int_0^\infty\int_0^\infty \frac{1}{k\,k_x}\left(e^{-k(z_0-z)} - e^{-k(z_0+z)}\right)\sin(k_x a)\cos(k_x\rho_x')$$

$$\cdot \sin(k_y b)\sin(k_y\rho_y')\,dk_x\,dk_y \qquad (A4)$$

for $0 \le z \le z_0$.

Using the identities

$$\sin(k_x a)\cos(k_x\rho_x') = \frac{1}{2}\left[\sin(k_x(a-\rho_x')) + \sin(k_x(a+\rho_x'))\right] \qquad (A5)$$

$$\sin(k_y b)\sin(k_y\rho_y') = \frac{1}{2}\left[\cos(k_y(b-\rho_y')) - \cos(k_y(b+\rho_y'))\right], \qquad (A6)$$

the expression for E_x splits up into 8 terms, each of which can be expressed in the form

$$e_x = -j\frac{\omega\mu_0 I}{2\pi^2}\int_0^\infty\int_0^\infty f_1(\pm z,\pm\rho_x')\left(\cos\left[k_y(b-\rho_y')\right]\right.$$

$$\left. - \cos\left[k_y(b+\rho_y')\right]\right)dk_x\,dk_y \qquad (A7)$$

where

$$f_1(\pm z,\pm\rho_x') = \frac{1}{k\,k_x}\sum^{sign} e^{-k(z_0 \pm z)}\sin\left[k_x(a\pm\rho_x')\right]. \qquad (A8)$$

The symbol $\sum^{sign}$ indicates that f_1 is a sum of all possible sign combinations of z and ρ_x' in the expression on the right-hand side of the equation. Integrating over k_y we see that the integral is a cosine transform that has the form and solution[A1] shown below for $0 \le z < z_0$.

$$\int_0^\infty (x^2+\alpha^2)^{-1/2} \exp\left[- \beta(x^2+\alpha^2)^{1/2}\right] \cos(xy)\, dx = K_0\left[\alpha(\beta^2+y^2)^{1/2}\right] \qquad (A9)$$

where

$$x = k_y,\ \alpha = k_x,\ \beta = z_0 \pm z,\ y = b \pm \rho_y' \quad ,$$

and $K_0(\ )$ is the modified Bessel function of the second kind of order zero.

The remaining integral is a sine tranform and has the form and solution[A2]

$$\int_0^\infty x^{-\lambda} K_\mu(ax) \sin(xy)\, dx = \frac{y\, \Gamma\left(\frac{1}{2}\mu - \frac{1}{2}\lambda + 1\right) \Gamma\left(1 - \frac{1}{2}\lambda - \frac{1}{2}\mu\right)}{2^\lambda c^{2-\lambda}}$$

$$\cdot\ {}_2F_1\left(\frac{2+\mu-\lambda}{2}\ ,\ \frac{2-\lambda-\mu}{2}\ ;\ \frac{3}{2}\ ;\ \frac{-y^2}{a^2}\right) \qquad (A10)$$

where

$$x = k_x,\ y = a \pm \rho_x',\quad a = \left[(b \pm \rho_y')^2 + (z_0 \pm z)^2\right]^{1/2} \quad ,$$

$$\lambda = 1,\quad \mu = 0 \quad ,$$

$\Gamma(\ )$ is the gamma function, and ${}_2F_1(\ )$ is a hypergeometric function. With the values of λ and μ given above, the hypergeometric function simplifies to[A3]

$${}_2F_1\left(\frac{1}{2},\ \frac{1}{2};\ \frac{3}{2};\ -t^2\right) = \frac{1}{t}\, \ell n\left(t + (1+t^2)^{1/2}\right) \qquad (A11)$$

with

$$t = \frac{a \pm \rho_x'}{\sqrt{(b \pm \rho_y')^2 + (z_0 \pm z)^2}} \quad .$$

Using the fact that $\Gamma(\frac{1}{2}) = \sqrt{\pi}$, the final form of E_x becomes that given in Eqs. 37 and 38.

Eqs. 23 and 24 show that, in the integration to obtain E_y, the role of k_x and k_y will be interchanged from that used in the integration for E_x. Hence, E_y can be obtained from E_x by performing the substitution given in Eq. 39, and changing the sign.

In deriving the expression for the magnetic field, it is convenient to start with Eq. 35 for H_y. Using manipulations similar to those used for E_x, the integration can be expressed as the following cosine transform[A4] in k_y:

$$\int_0^\infty \exp(-\beta(x^2 + \alpha^2)^{1/2}) \cos(xy)\, dx = \alpha\beta(y^2 + \beta^2)^{-1/2}\, K_1\left[\alpha(y^2 + \beta^2)^{1/2}\right] \tag{A12}$$

where the parameters are the same as those given in connection with Eq. A9, and $K_1(\ )$ is the modified Bessel function of the second kind of order one. The integration over k_x involves the sine transform[A5]

$$\int_0^\infty K_\nu(ax) \sin(xy)\, dx = \frac{1}{4}\pi a^{-\nu} \csc(\tfrac{1}{2}\nu\pi)(a^2 + y^2)^{-1/2}$$

$$\cdot \left\{\left[(y^2 + a^2)^{1/2} + y\right]^\nu - \left[(y^2 + a^2)^{1/2} - y\right]^\nu\right\} \tag{A13}$$

where $\nu = 1$, $a = [(b \pm \rho_y')^2 + (z \pm z_0)^2]^{1/2}$, and $y = a \pm \rho_x'$. Using this result, the y component of the magnetic field can be written as shown in Eqs. 41 and 42. H_x is obtained using the same substitution that is used to convert the equation for E_x to that for E_y.

REFERENCES

FOR APPENDIX A

A1. A. Erde'lyi (Ed.), Tables of Integral Transform, Vol. 1, p. 17 formula 27, McGraw-Hill Book Company, New York 1954.

A2. Ibid, p. 106, formula 50.

A3. M. Abramowitz and I. A. Stegun (Eds.), Handbook of Mathematical Function, p. 556, 15.1.7, National Bureau of Standarts, Washington 1972.

A4. A. Erde'lyi (Ed.), Tables of Integral Transforms, Vol. 1, p. 16, formula 26, McGraw-Hill Book Compnay, New York 1954.

A5. Ibid, p. 105, formula 48.

APPENDIX B

PROJECT INTERACTIONS

A. Interactions

1. A. J. Bahr, "Electromagnetic Sensor Arrays--Experimental Studies," presented at the AFML/AFOSR contract review of NDE research, Ames Laboratory, University of Iowa, Ames, IA, April, 1985.

2. A. J. Bahr, "Electromagnetic Sensor Arrays--Experimental Studies," presented at the review of Progress in Quantitative NDE, Williamsburg, VA, June, 1985, and published in the conference proceedings.

3. B. A. Auld and A. J. Bahr, "A Novel Multifunction Robot Sensor," presented at the 1986 IEEE International Conference on Robotics and Automation, San Francisco, California, April 1986, and published in the conference proceedings.

4. A. Rosengreen and A. J. Bahr, "Inductive Sensor Arrays for NDE and Robotics," presented at the Review of Progress in Quantitative NDE, La Jolla, California, August 1986, and published in the conference proceedings.

5. A. Rosengreen, A. J. Bahr, and D. M. Marsland, "Inductive Arrays for Near-Field Edge Tracking and Ranging," presented at the Review of Progress in Quantitative NDE, Williamsburg, VA, June 1987, and published in the conference proceedings.

6. A. J. Bahr participated in the TTCP Workshop on Field-Flaw Modeling in Electromagnetic NDE, Dayton, OH, August 1987.

7. A. J. Bahr, "Electromagnetic Theory of Eddy-Current Imaging," to be published.

B. Personnel

Dr. A. J. Bahr, Staff Scientist and Principal Investigator

Ms. D. M. Marsland, Research Engineer

Mr. A. Rosengreen, Sr. Research Engineer

Mr. W. B. Weir, Sr. Research Engineer

C. Acknowledgement

The authors thank Professor B. A. Auld and Dr. M. Gimple of Stanford University for many helpful discussions, Mr. K. Reeds for constructing the sensor array and its associated electronics, and Dr. R. Warren for guidance on the Fourier transform and the numerical integration.

REFERENCES

1. M. Gimple and B. A. Auld, "Position and Sample Feature Sensing with Capacitive Array Probes," presented at the Review of Progress in Quantitative NDE, Williamsburg, VA (June 1987).

2. A. Rosengreen and A. J. Bahr, " Inductive Sensor Arrays for NDE and Robotics," Review of Progress in Quantitative Nondestructive Evaluation, Vol. 6A, pp. 745-750, D. O. Thompson and D. E. Chimenti, editors, Plenum Press, New York (1987).

3. C. V. Dodd and W. E. Deeds, "Analytical Solutions to Eddy-Current Probe-Coil Problems," J. Appl. Phys., Vol. 9, pp. 2829-2839 (May 1968).

4. R. E. Beissner and M. J. Sablick, "Summary of Image Theory of Eddy Currents Induced by a Nonsymmetric Coil Above a Conducting Half-Space," J. Appl Phys., Vol. 56, pp. 448-454 (July 1984).

5. P. R. Bannister, "Summary of Image Theory Expressions for the Quasi-Static Fields of Antennas at or Above the Earth's Surface," Proc. IEEE, Vol. 67, pp. 1001-1008 (July 1979).

6. D. J. Thompson and J. T. Weaver,"Image Approximation for Quasi-Static Fields Over a Two-Layer Conductor," Elect. Ltrs., Vol. 6, pp. 855-856 (1970)

7. B. A. Auld, F. G. Meunnemann, and M. Riaziat, "Quantitative Modelling of Flaw Responses in Eddy Current Testing," Research Techniques in Nondestructive Testing, Vol. 7, pp. 37-76, R. S. Sharpe, editor Academic Press, London (1984).

8. B. A. Auld, J. Kenny, and T. Lookabaugh, "Electromagnetic Sensor Arrays--Theoretical Studies," Review of Progress in Quantitative Nondestructive Evaluation, Vol. 5A, pp. 681-690, (1985).

9. A. J. Bahr and D. W. Cooley, "Analysis and Design of Eddy-Current Measurement Systems, Review of Progress in Quantitative Nondestructive Evaluation, Vol. 2A, pp. 225-244 (1983)

END

DATE

FILMED

5-88

DTIC